Applied Catalysis B: Environmental 150–151 (2014) 459–465

Contents lists available at ScienceDirect

Applied Catalysis B: Environmental

journal homepage: www.elsevier.com/locate/apcatb

In situ XAS study of an improved natural phosphate catalyst for hydrogen production by reforming of methane

Moctar O. Abba[a,b], Victor M. Gonzalez-DelaCruz[a], Gerardo Colón[a], Said Sebti[b], Alfonso Caballero[a,*]

[a] Instituto de Ciencia de Materiales de Sevilla (CSIC-University of Seville) and Dep. de Quimica Inorganica, University of Seville, Avda. Américo Vespucio, 49, 41092 Seville, Spain

[b] Laboratoire de Chimie Organique Catalyse et Environnement (URAC 17), Université Hassan II Mohammedia-Casablanca, Faculté des Sciences Ben M'Sik, BP 7955, 20702 Casablanca, Morocco

ARTICLE INFO

Article history:
Received 24 October 2013
Received in revised form
10 December 2013
Accepted 16 December 2013
Available online 22 December 2013

Keywords:
Nickel catalysts
Natural phosphate
XAS
TPR
Methane reforming
Mechano-chemical catalysis

ABSTRACT

Some nickel catalysts supported on natural phosphate (NP) have been tested for the dry methane reforming reaction. Although the original impregnated 15%Ni/NP catalyst has no activity at all, the modification of the support by mechano-chemical and/or acid treatment strongly improved the catalytic performance, yielding a series of very active and stable catalysts. The chemical and physical characterization by X-ray diffraction (XRD), temperature programmed reduction (TPR), in situ X-ray absorption spectroscopy (XAS) and other techniques have shown that these treatments mainly modify the interaction between the nickel phase and the support surface. The nickel ions occupy calcium position in the surface of the phosphate phase, which stabilizes and improves the dispersion of nickel species. The final reduced catalysts present a much better dispersed metallic phase interacting with the NP surface, which has been identified as responsible for the observed outstanding catalytic performances.

1. Introduction

The production of hydrogen and synthesis gas from natural gas is a first order priority in the international energy policies. Nowadays, the main industrial reaction for obtaining hydrogen is the steam reforming reaction of methane, the main component of natural gas. As during the last decade the number of natural gas fields has hugely increased, the reserves and price of this chemical has decreased and it is expected to be severely reduced in the next decades [1,2]. Although it is well known that various transition and noble metals have high catalytic performances for reforming of methane, nickel containing catalytic systems are widely used for this hydrocarbon reforming reaction, mainly due to the low price and acceptable catalytic performance for the production of hydrogen [3–6]. Beside this reaction, the dry reforming of methane (DRM), using carbon dioxide as oxidant, has attracted very much attention as an alternative reaction. Although some authors have pointed out that it is impractical for commercial hydrogen generation [7], the DRM has additional environmental and industrial interest, as it can be used to valorize and/or eliminate the CO_2 from natural gas deposits. Even more, the use of two greenhouse gases (methane and CO_2) for obtaining hydrogen and synthesis gas (CO/H_2), which is one of the main chemicals currently used in major industrial processes as methanol synthesis, hydrogenations or Fischer–Tropsch reactions [8–10], has an unquestionable environmental interest.

The main issue related with the use of these Ni-based materials as catalysts is their low resistance to the coke deposition during reaction, which requires introducing regeneration steps during the catalytic process, hindering their use as a long term catalyst in industrial applications. It is well known that factors as the dispersion of the metallic phase onto the support, the morphology of the metallic particles or the interaction of these nickel metallic particles with the surface of the support are important factors determining the catalytic activity and stability of these catalysts [11–16]. In general, the preparation of well-dispersed Ni-based catalysts is not an easy task. Therefore, the choice of the support is one of the main factors affecting the stability of the Ni-based catalysts, and a great number of them have been studied by different authors [9,15,17–19]. Natural phosphate (NP), mainly obtained from an ore in Morocco (more than 75% of world reserves) has been used as catalysts in a wide range of catalytic reactions involving different types of organic reactions [20–22]. In this work, we have explored the application of NP as a support for nickel catalysts in the aforementioned reforming reactions as much as obtained from the ore

* Corresponding author. Tel.: +34 627439545.
E-mail address: caballero@us.es (A. Caballero).

0926-3373/$ – see front matter © 2013 Elsevier B.V. All rights reserved.
http://dx.doi.org/10.1016/j.apcatb.2013.12.031

as modified by different chemical and mechanical treatment. The use of different characterization techniques, as XRD, SEM or in situ XAS, has allowed us to determine and chemical and physical state of the nickel particles achieved under different preparation conditions and nickel content, namely 15 wt% and 3 wt% Ni/NP catalytic systems. As the former systems have a rather high nickel content, the 3 wt% Ni systems have allow us to study in details the interaction between the nickel phase and the support surface, mainly by XAS techniques.

2. Experimental

2.1. Catalysts preparation

Natural phosphate (NP) came from an extracted ore in the region of Khouribga (Morocco). The fraction of 100–400 μm grain size was washed with water, calcined at 900 °C for 2 h, washed again, calcined again at 900 °C for 0.5 h and ground (63–125 μm fraction). As in other previous works on the same support [21,22], the structure of NP is similar to that of carbonate hydroxyfluorapatite as shown by X-ray diffraction pattern and chemical analysis. Details about these treatment and elemental analysis can be found in the aforementioned works [21,22].

This NP phosphate support was then modified by two different treatments. So, a fraction of NP was submitted to a treatment with nitric acid 1 M. After contacting the powder during 2 h, the so prepared NP—H sample was water washed and dried at 120 °C. Alternatively, the NP was submitted to a ball milling mechanochemical treatment during 20 and 60 min, respectively. This kind of ball milling treatment was initially developed for diminishing its particle size. However, it has become during the last decade in a green chemistry method for synthesizing a large number of nanosized materials avoiding the use of solvents [23]. Even more, some previous works have shown it can improve the performance of different catalytic systems [24]. The samples have been ground by means of a high grinding energy ball mill SPEX, model Mixer mill 8000 M. Both grinding jars and balls made of hardened steel have been used. The volume of the jar was 50 cc with an internal diameter of 38 mm. Sample amounts of 3 g were ground using 5 balls with 12 mm in diameter in the whole set of grinding experiments. The powder to ball mass ratio was always closed to 1:12. The clamp speed of the shaker mill was 875 cycles/min. The supports obtained by this treatment were denoted as NP-B20, NP-B60, NP—H-B20 and NP—H-B60, indicating that the original or the acid treated phosphates were ball milled during 20 or 60 min. In both cases, no changes in the elemental composition of the NP were observed after the treatments.

As indicated in Section 1, two different nickel loadings were used, namely a 3 wt% and a 15 wt% Ni on NP, NP—H, NP—H-B20 and/or NP—H-B60. These nickel catalysts were prepared by aqueous slurry impregnation using a nickel acetate solution $Ni(CH_3COO)_2$. The mixture was stirred at room temperature for 1 h, the slurry was dried at 120 °C in a sand bath, kept overnight at 120 °C in an oven, heated to 400 °C with a 1 °C/min ramp rate, and calcined in air at 400 °C for 2 h.

2.2. Catalytic activity tests

Dry reforming of methane reaction (DRM) was carried out in a fixed-bed tubular reactor described elsewhere [25], using 40 mg of catalysts between two pompons of quartz wool. Before reaction, samples were reduced with H_2 at 500 °C during 1 h. The CH_4 and CO_2 reactants were mixed at a ratio of 1 diluted in He (10:10:80 in volume). The samples were heated from room temperature up to 750 °C at 1 °C/min rate, held at 750 °C during 12 h, and finally cooled down to room temperature in the same reaction mixture. All reactives and products were analyzed by means of a gas chromatograph (Varian, CP-3800) equipped with a thermal conductivity detector (TCD) and a Porapak Q packed column.

2.3. Temperature programmed reduction (TPR)

TPR experiments were done from room temperature up to 750 °C, with a heating rate of 10 °C/min. A thermal conductivity detector (TCD), previously calibrated using CuO, and a mass spectrometer in line with the TCD, calibrated with reference mixtures, were used to detect variations of reducing agent concentration, and possible sub-products formation. A H_2/Ar mixture (5% H_2, 50 ml/min flow) was used for H_2-reduction. All the experimental conditions were chosen to assure that no peak coalescence occurs, according to the conditions indicated in Ref. [26].

2.4. X-ray diffraction (XRD), textural properties and scanning electron microscopy (SEM)

X-ray diffractograms were recorded in a Panalytical XPert PRO device, equipped with an X'Celerator Detector (active range of $2\theta = 2.18°$), with a Bragg–Brentano configuration, using Cu $K\alpha$ ($\lambda = 1.5418$ Å). General diagrams were collected in the range $2\theta = 20°–80°$, with a step of 0.05° and an acquisition time of 80 s for each point. The mean size of the crystalline particles of nickel and support phases was calculated by the Scherrer formula. X-ray diffractograms were also collected in the range of $2\theta = 35°–55°$, with a step of 0.03° during 100 s each point. The textural properties of solids (specific surface area) were determined from nitrogen adsorption–desorption isotherms at liquid nitrogen temperature by using a Micromeritics ASAP-2010 instrument. Surface areas were calculated by the BET method. Prior to measurements, all samples were degassed at 110 °C to 0.1 Pa. SEM images were obtained in a Hitachi S-5200 microscopy equipped with a field emission filament, using an accelerating voltage of 5 kV.

2.5. X-ray absorption spectroscopy

X-ray absorption spectra (XAS) were recorded at the BM25 beam line (SPLINE) of the ESRF synchrotron (Grenoble, France). The spectra were acquired in transmission mode, using self-supported wafers of the Ni supported samples, in a modified commercial infrared cell (Specac) able to work up to 800 °C under controlled atmosphere [27]. XAS spectra were collected at different temperatures during treatments of the samples.

In all cases the self-supported pellets were prepared using the optimum weight to maximize the signal-to-noise ratio in the ionization chambers ($\log I0/I1 \approx 1$). Mass flow controllers were used for dosing the gases to the cell. The composition of the gas mixtures was similar to that previously used in the TPR experiment during the hydrogen treatments. The energy calibration was accomplished using a standard Ni foil introduced after the second ionization chamber ($I1$). Typical XAS spectra of Ni K-edge were recorded from 8200 to 9100 eV, with a variable step energy value, with a minimum 0.5 eV step across the XANES region. Once extracted from the XAS spectra, the EXAFS oscillations were Fourier transformed in the range 2–11.0 $Å^{-1}$. Spectra were analyzed using the software package IFEFFIT [28]. The theoretical paths for Ni—Ni and Ni—O species used for fitting the first coordination shell of the experimental data were generated using the ARTEMIS program and the FEFF 7.0 program [29]. The coordination number, interatomic distance, Debye–Waller factor and inner potential correction were used as variable parameters for the fitting procedures. Reference spectra

Table 1
Specific surface areas obtained by the BET method and crystallite size (Scherrer formula) for the different supports and Ni-based catalysts.

	S_{BET} (m^2/g)	Crystallite size (nm)
NP	<1.0	360
NP—H	<1.0	350
NP—H-B20	4.8	225
NP—H-B60	15.6	155
15%Ni/NP—H	9.2	350
15%Ni/NP—H-B20	19.1	220
15%Ni/NP—H-B60	35.0	155

for metallic Ni and NiO were recorded using standard reference samples.

3. Results and discussion

3.1. Structural and surface properties of original and modified NPs

The crystalline phases present in the original and acid and milled modified NP supports were analyzed using X-ray diffraction. XRD patterns of every sample (not shown) contain the peaks characteristic of carbonate fluoroapatite, as found in previous related works [21]. Both, the acid and milled treatment maintain the same XRD patterns, although the milled samples present diffraction peaks a bit widener, compatible with a slight amorphization of the NP solids. These results are consistent with the crystalline size and BET surface areas obtained for the different supports (Table 1). So, while NP and NP—H have BET values lower than 1 m^2/g, with crystalline sizes of about 350 nm, the ball milled samples present much higher values, until 15.6 m^2/g for the NP—H-B60 support, decreasing the crystallite size down to 225 (NP-B20) and 155 nm (NP-B60), respectively. Also, an important increase in the BET areas is observed when a 15%wt Ni is deposited onto the supports, reaching the 15 wt% Ni/NP—H-B60 sample a value of 35 m^2/g. However, no changes are observed when a 3 wt% Ni is loaded in the different supports (data not included).

3.2. Catalytic performances in the dry reforming reaction of methane (DRM)

We have studied the catalytic performance of the Ni/NP catalysts submitted to the different activation processes. None of the 3 wt%/NP catalysts show catalytic activity in the whole range of studied temperature (until to 750 °C). Likewise, the 15 wt% Ni catalytic systems supported on NP, NP-B20 or NP-B60 without, respectively, the ball milling or the acid treatment were inactive for the DRM. However, as shown in Fig. 1, after the acid treatment of the NP support, the 15%Ni/NP—H catalysts presents a high initial activity, with a 62% methane conversion at 750 °C. The higher conversion observed for CO_2 (72%) indicates some contribution of the inverse water–gas shift reaction. Nevertheless, this catalytic system presents a relatively low stability, as after 30 h in stream the conversion of methane decrease to about 25%.

The same NP—H support submitted to a mechano-chemical treatment yields catalysts extremely active and stable. As it can be seen in Fig. 2, after a treatment of 20 (NP—H-B20) and 60 (NP—H-B60) min, the initial methane conversions are in both cases higher than 84%, with some losses of activity after 7 h of reaction for both catalysts although much lower for the B20 system.

So, these results show as the modification of the support by two different treatments, namely acid and mechano-chemical treatment, turn an inactive catalyst into a very performance system, remarkable from the point of view of activity and stability. As the active sites in the reforming reactions of methane are the surface of

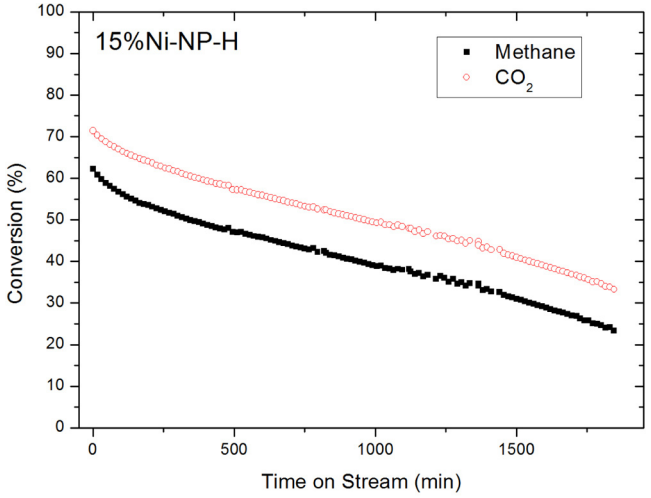

Fig. 1. CH_4 and CO_2 conversions in the reaction of DRM ($CH_4 + CO_2 \rightarrow 2H_2 + 2CO$) at 750 °C, using 15 wt% Ni—NP—H catalyst.

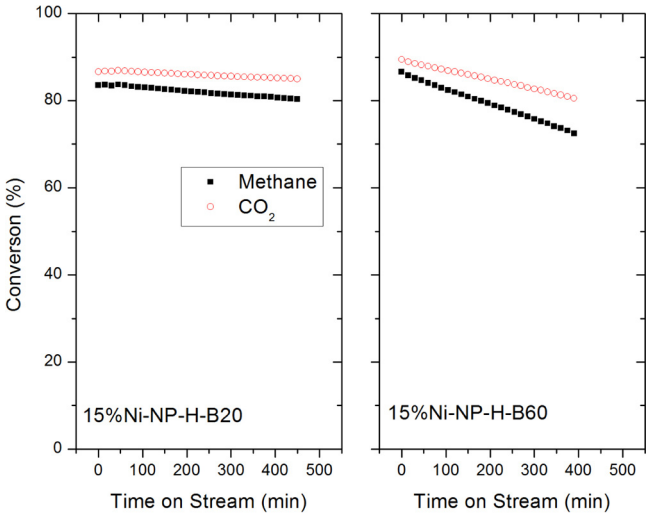

Fig. 2. CH_4 and CO_2 conversions in the reaction of DRM at 750 °C, using 15 wt% Ni—NP—H-B20 (left) and 15 wt% Ni—NP—H-B60 catalysts (right).

the metallic nickel particles, these treatments must have dramatically changed the state and interaction of the nickel phase with the NP support. In order to understand the origin of these outstanding properties, we have characterized the NP support and the nickel metallic phase by means of different chemical and physical techniques.

3.3. Chemical characterization of 15 wt% Ni/NPs catalysts

The nickel metallic phase of the different catalytic systems has been studied by temperature programmed reduction (TPR). As shown in Fig. 3, when supported in the original NP without any further treatment (red line), the reduction profile of nickel presents a main peak centered at about 375 °C, and a shoulder at higher temperature, in a similar range to that observed for the NiO used as a reference (red line). So, the 15 wt% Ni/NP catalyst is easier to reduce than the NiO, probably as a consequence of the dispersion on the support. The acid treatment of the NP increases this effect as the 15 wt% Ni/NP—H (black line) has now the main peak centered at 340 °C. As this acid treatment does not change the BET surface or the crystalline size of support, this result can be taken as evidence that this treatment just produces a modification of the support

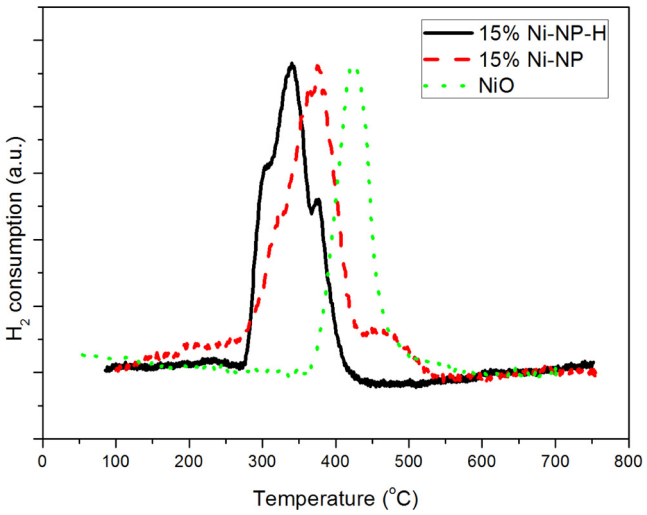

Fig. 3. TPR profiles of 15 wt% Ni—NP and 15 wt% Ni—NP—H catalysts. (For interpretation of the references to color in text, the reader is referred to the web version of the article.)

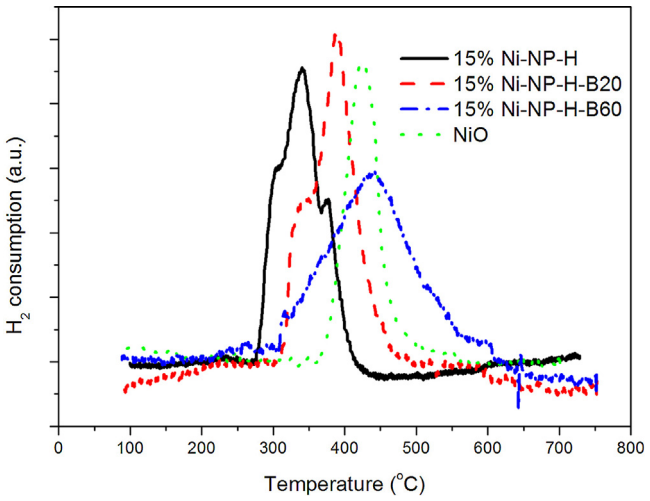

Fig. 5. TPR profiles of 15 wt% Ni—NP—H catalyst and the analogous submitted to a ball-milled treatment (B20 and B60 samples). (For interpretation of the references to color in text, the reader is referred to the web version of the article.)

surface, probably creating surface vacancies and other defects, which favors the dispersion of the nickel phase.

By comparing SEM images of both catalysts (Fig. 4), it appears that the nickel particles supported on NP—H (right), looking like warts when compared with the support images (not shown), have a more spongy appearance, which can account for the higher activity and lower reduction temperature. These images also explain the higher value of BET area obtained when the nickel is supported in the acid treated NP—H (Table 1).

The effect of the mechanical treatment in the TPR profile is shown in Fig. 5. It can be seen as after 20 min milling, the nickel phase is now less reducible (red line), with reduction temperatures similar to the untreated 15 wt% Ni/NP, but still lower than the NiO reference. It is worth to note that although the reduction temperature range of the untreated 15% Ni/NP is similar to that of the B20 milled sample, their catalytic activity are pretty different. So, these facts are showing as different chemical state of the nickel dispersed phases can present similar TPR profile. In this case, the lower reduction temperature of the untreated sample compared to a NiO phase must come from the increase in the dispersion state. On the contrary, this dispersed phase in the 15 wt% Ni/NP—H-B20 catalyst, interacting differently with the NP—H support, seems to revert the effect, now reducing at a higher temperature. The same effect is observed for the 60 min milled 15 wt% Ni/NP—H-B60 catalysts, which reduces even at a higher temperature, in such a way that the reduction processes is completed only at 600 °C. As shown before (Table 1) the specific surface of the nickel phase in the milled systems is dramatically enlarged, and simultaneously, the crystalline size of the support is decreased by the B60 treatment. So, the increase in the reduction temperature by milling treatment must come from a bigger interaction with the activated support.

According to the literature [30,31] these high temperature reduction processes can be ascribed to nickel ions substituting Ca(II) in the fluoroapatite structure of the NP. Since no phase with nickel and calcium can be identified by XRD (in fact, no calcium–nickel phosphate phases can be found in JCPDS and other reports) this must be a kind of surface mixed phase, where the nickel is incorporated to the fluoroapatite structure. As extensively discussed in Ref. [30], the existence of a chemically similar strontium nickel phosphate reported in a previous work [32] supports the hypothesis that this new surface nickel phase is present in the ball-milled samples. This treatment, increasing the BET area and decreasing the crystalline sizes (Table 1), must produce an important number of defects and structural disorder in the surface of the NP support, facilitating the incorporation of nickel to the fluoroapatite structure.

This point is also confirmed by the SEM images showed in Fig. 6. The 15 wt% Ni/NP—H-B20 sample presents well dispersed nickel particles (the wart-looking particles cannot be detected), while the nickel in the 15 wt% Ni/NP—H-B60 seems to be covered by the NP support, indicating a strong interaction with the support. This could accounts for the lower catalytic stability observed for this sample. At this point, it is worth noting that the DRM reaction is a very demanding one, mainly because the high reaction temperature, which favors the agglomeration of metallic particles. So, the big interaction between nickel and support, stabilizing the

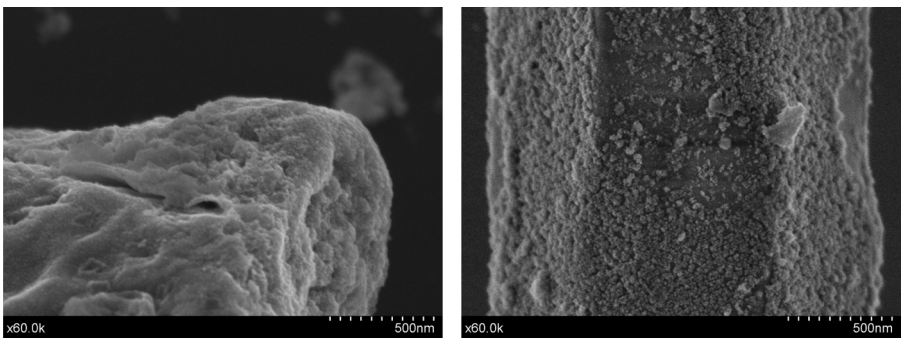

Fig. 4. SEM images of the calcined 15 wt% Ni—NP (left) and 15 wt% Ni—NP—H (right) catalysts.

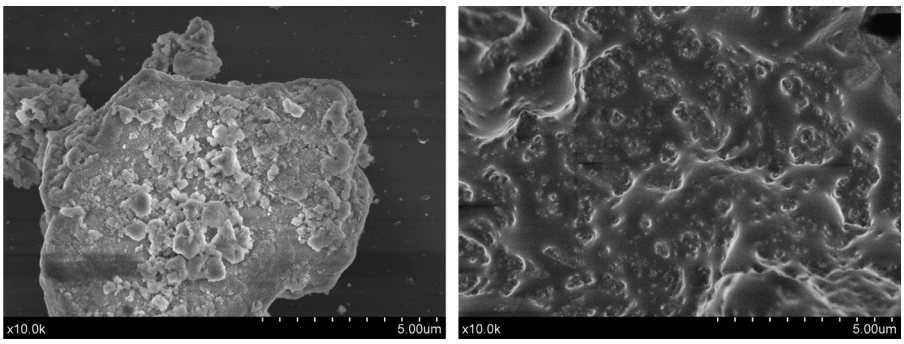

Fig. 6. SEM images of the calcined 15 wt% Ni—NP—H-B20 (left) and 15 wt% Ni—NP—H-B60 (right) catalysts.

metallic particles, could accounts for the higher catalytic stability of the 15 wt% Ni/NP—H-B20 system. In the case of the 15 wt% Ni/NP—H-B60, this interaction is so strong that seems to bury the nickel in the subsurface region of the support, hindering the access to the nickel active sites.

3.4. X-ray absorption spectroscopy (XAS)

To shed light on the chemical and physical state of the nickel phases on the different treated supports, an in situ X-ray absorption spectroscopy study have been accomplished. However, in all samples with a nickel content of 15 wt%, the reduction treatment gives raise to nickel particles with coordination numbers of 12, which restrict the usefulness of XAS for the characterization of these systems, especially regarding to the interaction of the nickel particles with the NP support. To overcome this issue, we have used catalytic systems prepared in a similar way, but just with a 3 wt% Ni content, which has allowed us a more in depth analysis of the nickel metallic phases, and especially in relation with the interaction with the surface of NP supports. In this way, the effect of the acid treatment and the 20 min milling on the 3 wt% Ni catalysts has been analyzed. In all cases, the spectra were collected in situ, within the environmental cell, in contact with reactive gases, and after cooling down to room temperature.

Fig. 7 includes the XANES spectra obtained for the calcined 3 wt% Ni/NP and 3%Ni/NP—H, respectively. Both spectra roughly correspond to a well-formed nickel oxide phase, similar to that obtained for a NiO Ref. [15]. On the contrary, differences are observed in the XANES spectra of the catalysts prepared with the PN-B20 supports (Fig. 8), where the 3 wt% Ni/NP-B20 sample has once again a XANES spectrum typical for a massive NiO phase, while the 3 wt% Ni/NP—H-B20 catalysts presents differences in the relative intensities of oscillations. These differences are more clearly reflected in the Fourier transform curves of Fig. 9. As shown, the B20 milled support gives rise to a F.T. dominated by two main peaks centered at 1.88 and 2.80 Å (without phase correction) whose relative intensities are characteristic of the cubic phase of NiO [25]. The interatomic distances (R) and coordination numbers (C.N.) obtained by fitting analysis of these curves (Table 2), very close to that of the NiO reference, confirm this assumption. However, it is evident from the figure that the second peak intensity of the 3 wt% Ni/NP—H-B20 catalyst, corresponding to the Ni—Ni second shell distances of the NiO phase, is much lower, resulting from the fitting procedure in a mean Ni—Ni second shell coordination number of 8.7 (Table 2). A value lower than 12 for this coordination shell is compatible with the existence of isolated, disordered and very tiny nickel oxide entities, which must be stabilized by strong interaction with the milled/acid treated NP support. This conclusion is also supported by the relatively high D–W factor values, especially for the acid treated catalysts, compatible with the existence of a pretty disordered oxide phase. At this point, it is worthy to note that the relatively big intensity of the second F.T. peak of NiO comes from

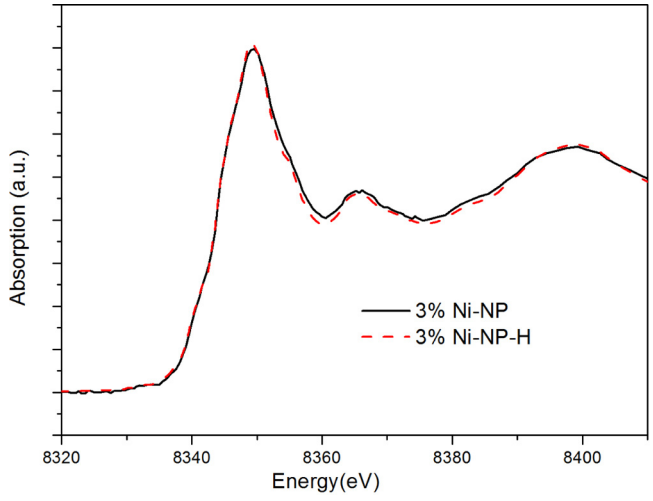

Fig. 7. In situ XANES spectra of the calcined 3 wt% Ni—NP and 3 wt% Ni—NP—H. All the spectra have been collected after cooling down at room temperature in contact with the gas phase.

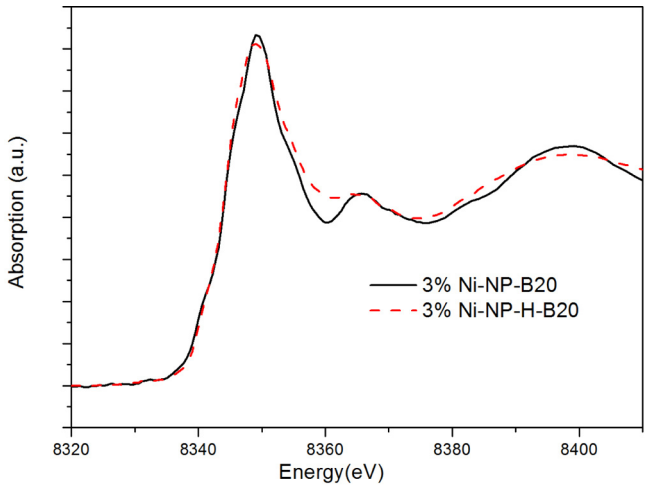

Fig. 8. In situ XANES spectra of the calcined 3 wt% Ni—NP-B20 and 3 wt% Ni—NP—H-B20. All the spectra have been collected after cooling down at room temperature in contact with the gas phase.

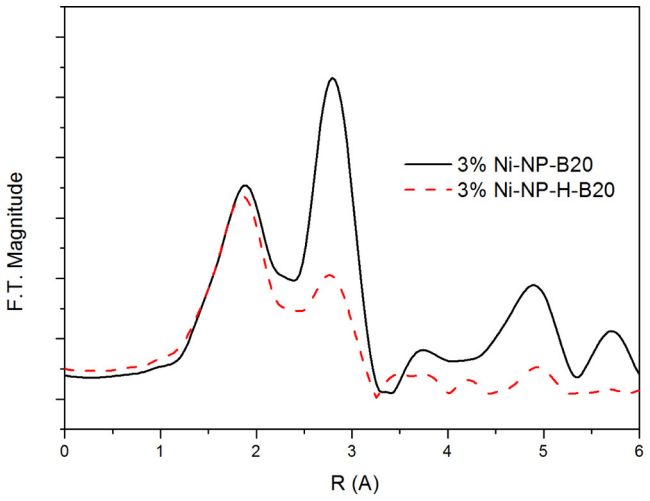

Fig. 9. Fourier transform functions of the EXAFS oscillations (without phase correction) obtained for the calcined 3 wt% Ni—NP-B20 and 3 wt% Ni—NP—H-B20. All the spectra have been collected after cooling down at room temperature in contact with the gas phase.

Table 2
Structural parameters for Ni obtained by fitting analysis of the EXAFS spectra of Ni/NP catalyst submitted to the indicated treatments.

	R (Å)	C.N.	D–W ($Å \times 10^{-3}$)	ΔE_0 (eV)
3 wt% Ni/NP-B20	2.09 (Ni—O)	6.1	5.9	−3.2
Calcined	2.97 (Ni—Ni)	11.3	10.8	
3 wt% Ni/NP—H-B20	2.06 (Ni—O)	5.3	5.0	−2.2
Calcined	2.99 (Ni—Ni)	8.7	21.2	−2.7
NiO	2.08 (Ni—O)	6.0	–	–
	2.95 (Ni—Ni)	12.0		
3 wt% Ni/NP-B20 Reduced	2.50 (Ni—Ni)	7.1	5.9	−2.4
3 wt% Ni/NP—H-B20 Reduced	2.50 (Ni—Ni)	4.9	5.4	−5.5
Ni foil	2.49 (Ni—Ni)	12.0	0.0	0.0

Estimated errors: interatomic distance < ±0.02 A; coordination number (C.N.) < ±10%.

a forward-scattering effect characteristic of cubic crystallographic phases where the first and second Ni—O—Ni coordination shell are aligned [33]. Therefore, a relatively amorphous nickel oxide phase, where this alignment has been partially lost, will yield a F.T. with a less intense second peak, even if the C.N. does not decrease. However, according to the TPR data of Section 3.3, another interpretation for this effect would be the formation of a new surface nickel calcium phosphate phase, which could also accounts for this effect.

To shed light on this point, a XAS study of the reduced 3 wt% Ni/NP-B20 and 3 wt% Ni/NP—H-B20 catalysts has been accomplished. In agreement with the TPR profile of Fig. 5, the F.T. obtained after reduction in hydrogen at 600 °C (Fig. 10) shows that both catalysts are reduced to metallic nickel. However, the peak centered at 2.39 Å (without phase correction), corresponding to Ni—Ni first coordination shell of metallic particles, is much smaller than the reference of nickel foil, especially in the 3 wt%/Ni/NP—H-B20 catalyst. The least-square fitting of these peak yields the data included in Table 2. The values of about 7 and 5 obtained for the C.N. of these two reduced samples show the presence of very tiny nickel metallic particle. More specifically, these values correspond to metallic clusters smaller than 1.5 and 1.0 nm in diameter respectively [34], showing the high dispersion, interaction of nickel phase with the treated NP support.

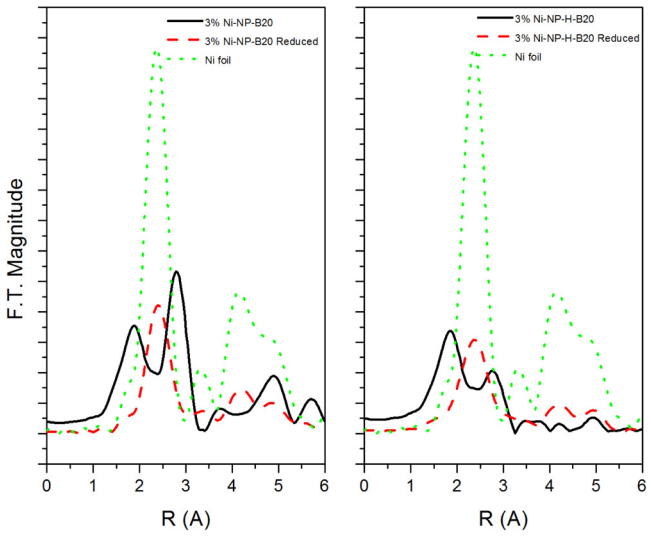

Fig. 10. Fourier transform functions of the EXAFS oscillations (without phase correction) obtained for the calcined and reduced 3 wt% Ni—NP-B20 and 3 wt% Ni—NP—H-B20. All the spectra have been collected after cooling down at room temperature in contact with the gas phase. A nickel foil function is included as a reference.

4. Conclusions

Nickel deposited on natural phosphate was found to be an inactive catalyst for the reforming reaction of methane. However, when modified by means of an acid and, specially, by a milled treatment, it appears as a very active and stable Ni-based catalyst. This important increase of the catalytic performance comes from several concurrent factors. First of all, the ball milling treatment produces a remarkable increase of the specific surface areas, and a parallel decrease of the crystalline size. But it also favors the interaction of the nickel metallic phase with support, with the formation of a new mixed phase of nickel and calcium at the NP surface. As a result, the reduced nickel particles appear as a well dispersed and anchored phase, improving both the initial activity but also the catalytic stability during the dry reforming of methane, that by avoiding the sintering of the metallic particles. So, these results show that the NP is an appropriated support for this industrial reaction and, maybe for many other catalytic formulations.

Acknowledgments

We thank the Ministry of Education and Science, the AECID of Spain and the European Union (FEDER funds) for financial support (Projects ENE2011-24412, AECID C/030491/10 and AECID A1/035614/11). We also thank the Moroccan MENESFCRS, CNRST (URAC 17, Project RS/2011/10) and OCP group. The help of ESRF facility and the BM25 Spline beamline staff is gratefully recognized.

References

[1] F.P. Wang, R.M. Reed, J.A. Jackson, K.G. Jackson, SPE Annual Technical Conference and Exhibition, New Orleans, Louisiana, 2009, ISBN 978-1-55563-263-2.
[2] G.E. King, SPE Annual Technical Conference and Exhibition, Florence, Italy, 2010, ISBN 978-1-55563-300-4.
[3] Y. Matsumura, T. Nakamori, Appl. Catal. 258 (2004) 107.
[4] W. Donga, H. Roha, K. Juna, S. Parka, Y. Ohb, Appl. Catal. A 226 (2002) 63.
[5] C. Batiot-Dupeyrat, G. Sierra Gallego, F. Mondragon, J. Barrault, J.M. Tatibouet, Catal. Today 107–108 (2005) 474–480.
[6] J.N. Armor, Appl. Catal. A 176 (1999) 159.
[7] D. Lee, P. Hacarlioglu, S.T. Oyama, Top. Catal. 29 (2004) 45.
[8] W.D. Zhang, B.S. Liu, Y.P. Zhan, Y.L. Tian, Ind. Eng. Chem. Res. 48 (2009) 7498.
[9] V.M. Gonzalez-Delacruz, F. Ternero, R. Pereñiguez, A. Caballero, J.P. Holgado, Appl. Catal. A: Gen. 384 (2010) 1.
[10] M. Balla, M. Wietschelb, Int. J. Hydrogen Energy 34 (2009) 615.

[11] J. Wei, E. Iglesia, J. Catal. 224 (2004) 370.
[12] K. Takehira, Catal. Surveys Jpn. 6 (2002) 19–32.
[13] R. Shiozaki, A.G. Andersen, T. Hayakawa, S. Hamakawa, K. Susuki, M. Shimizu, K. Takehira, Stud. Surf. Sci. Catal. 110 (1997) 701.
[14] G.C. Araujo, S.M. Lima, J.M. Assaf, M.A. Peña, J.L.G. Fierro, M.C. Rangel, Catal. Today 133 (2008) 129–135.
[15] V.M. Gonzalez-DelaCruz, J.P. Holgado, R. Pereñiguez, A. Caballero, J. Catal. 257 (2008) 307.
[16] M.M. Barroso-Quiroga, A.E. Castro-Luna, Int. J. Hydrogen Energy 35 (2010) 6052.
[17] R. Pereñíguez, V.M. González-DelaCruz, A. Caballero, J.P. Holgado, Appl. Catal. B 123 (2012) 324.
[18] V.M. Gonzalez-DelaCruz, R. Pereñiguez, F. Ternero, J.P. Holgado, A. Caballero, J. Phys. Chem. C 116 (2012) 2919.
[19] A. Caballero, J.P. Holgado, V.M. Gonzalez-delaCruz, S.E. Habas, T. Herranz, M. Salmeron, Chem. Commun. 46 (2010) 1097.
[20] S. Sebti, M. Zahouily, H.B. Lazrek, J.A. Mayoral, D.J. Macquarrie, Curr. Org. Chem. 12 (2008) 203.
[21] F. Bazi, H. El Badaoui, S. Tamani, S. Sokori, L. Oubella, M. Hamza, S. Boulaajaj, S. Sebti, J. Mol. Catal. A: Chem. 256 (2006) 43.
[22] J. Hidalgo-Carrillo, J. Sebti, M.A. Aramendia, A. Marinas, J.M. Marinas, S. Sebti, F.J. Urbano, J. Colloid Interface Sci. 344 (2010) 475.
[23] A. Perejón, N. Masó, A.R. West, P.E. Sánchez-Jiménez, R. Poyato, J.M. Criado, L.A. Pérez-Maqueda, J. Am. Ceram. Soc. 96 (2013) 1220.
[24] E. Manova, T. Tsoncheva, D. Paneva, I. Mitov, K. Tenchev, L. Petrov, Appl. Catal. A 277 (2004) 119.
[25] R. Pereñíguez, V.M. González-DelaCruz, J.P. Holgado, A. Caballero, Appl. Catal. B 93 (2010) 346.
[26] P. Malet, A. Caballero, J. Chem. Soc. Faraday Trans. I 84 (1988) 2369.
[27] A. Caballero, J.J. Morales, A.M. Cordon, J.P. Holgado, J.P. Espinos, A.R. Gonzalez-Elipe, J. Catal. 235 (2005) 295.
[28] M. Newville, J. Synchrotron Rad. 8 (2001) 322.
[29] B. Ravel, J. Alloys Compd. 401 (2005) 118.
[30] J.H. Jun, T. Lee, T.H. Lim, S. Nam, S. Hong, K.J. Yoon, J. Catal. 221 (2004) 178.
[31] Z. Boukha, M. Kacimi, M.F.R. Pereira, J.L. Faria, J.L. Figueiredo, M. Ziyad, Appl. Catal. A: Gen. 317 (2007) 299.
[32] A.A. Belik, B.I. Lazoryak, K.V. Pokholok, T.P. Terekhina, I.A. Leonidov, E.B. Mitberg, V.V. Karelina, D.G. Kellerman, J. Solid State Chem. 162 (2001) 113.
[33] B. Lengeler, Phys. Rev. Lett. 53 (1984) 74.
[34] A.I. Frenkel, C.W. Hills, R.G. Nuzzo, J. Phys. Chem. B 105 (2001) 12689.